

Control of Photochemical, Photophysical, Electrochemical, and Photocatalytic Properties of Rhenium(I) Complexes Using Intramolecular Weak Interactions between Ligands

Hideaki Tsubaki,[†] Akiko Sekine,[‡] Yuji Ohashi,[‡] Kazuhide Koike,[§]
Hiroyuki Takeda,[†] and Osamu Ishitani^{*,†}

Contribution from the Department of Chemistry and Department of Chemistry and Materials Science, Graduate School of Science and Engineering, Tokyo Institute of Technology, Ookayama 2-12-1, Meguro-ku, Tokyo, 152-8551, Japan, and National Institute of Advanced Industrial Science and Technology, Onogawa 16-1, Tsukuba 305-8569, Japan

Received June 10, 2005; E-mail: ishitani@chem.titech.ac.jp

Abstract: Intramolecular interactions between ligands have been successfully applied as a novel tool for controlling various properties of a series of *cis,trans*-[Re(dmb)(CO)₂(PR₃)(PR'₃)]⁺-type complexes (dmb = 4,4'-dimethyl-2,2'-bipyridine), in the ground state and in the excited state and in the one-electron reduced form. For rhenium complexes with two triarylphosphine ligands, P(*p*-XPh)₃, the dmb ligand was sandwiched by four aryl rings having CH(aryl)- π (pyridine)- π (aryl) interactions. On the other hand, complexes with one triarylphosphine ligand and one trialkylphosphite ligand, P(OR)₃, had π - π and CH- π interactions between each pyridine ring in the dmb ligand and the aryl group in the P(*p*-XPh)₃. Various properties of these two series of rhenium complexes were compared with those of complexes having two trialkylphosphite ligands, which do not interact through space with the dmb ligand. Properties of the complexes associated mainly with the dmb ligand are strongly affected by the intramolecular interactions: (1) UV/vis absorptions to the π - π^* and ¹MLCT excited states were both red-shifted, but (2) emission from the ³MLCT excited state was blue-shifted; (3) the lifetime of the ³MLCT excited state was prolonged up to 3-fold; (4) the reduction potential in the ground state was positively shifted by 110 mV with π - π and CH- π interactions and by 180–200 mV with the CH- π - π interactions. (5) In the excited states, the oxidation power of the complex was also enhanced by the intramolecular interactions. (6) In the corresponding one-electron-reduced species *cis,trans*-[Re(dmb^{-•})(CO)₂(PR₃)(PR'₃)], the intramolecular interactions are maintained and strongly affected their UV/vis spectra. (7) Photocatalysis for CO₂ reduction was significantly enhanced only by the CH- π - π interaction.

Introduction

Control of photochemical, photophysical, and electrochemical properties of transition metal complexes is of great interest because of the advantages of these complexes in fields of chemistry as diverse as photo- and electrocatalysts,^{1–3} photonic sensors,⁴ photochemical energy and electron transfer,^{1,5} chemi- and electroluminescence,⁶ molecular electronics, and photonics.^{5b,7} In the past two decades, d⁶ transition metal diimine

complexes including Ru(II), Ir(III), Pt(II), and Re(I) have been studied intensively in applications as a light absorber, which has been sought to absorb a wider energy range of solar light, and also as an emitter, which must have high quantum yield of emission, in light-harvesting⁸ and electroluminescent devices.⁶

[†] Department of Chemistry, Tokyo Institute of Technology.

[‡] Department of Chemistry and Materials Science, Tokyo Institute of Technology.

[§] National Institute of Advanced Industrial Science and Technology.

- (1) *Photosensitization and Photocatalysis Using Inorganic and Organometallic Compounds*; Kalyanasundaram, K., Graetzel, M., Eds; Kluwer Academic Publishers: Boston, 1993.
- (2) (a) Fujita, E.; Brunschwig, B. S.; Ogata, T.; Yanagida, S. *Coord. Chem. Rev.* **1994**, *132*, 195–200. (b) Sutin, N.; Creutz, C.; Fujita, E. *Comments Inorg. Chem.* **1997**, *19*, 67–92.
- (3) (a) Johnson, F. P. A.; George, M. W.; Hartle, F.; Turner, J. J. *Organometallics* **1996**, *15*, 3374. (b) Christensen, P.; Hamnett, A.; Muir, A. V. G.; Timney, J. A. *J. Chem. Soc., Dalton Trans.* **1992**, 1455.
- (4) (a) Demas, J. N.; DeGraff, B. A. *Coord. Chem. Rev.* **2001**, *211*, 317–351. (b) Kunugi, Y.; Mann, K. R.; Miller, L. L.; Exstrom, C. L. *J. Am. Chem. Soc.* **1998**, *120*, 589–590. (c) Yam, V. W. W.; Wong, K. M.-C.; Zhu, N. *J. Am. Chem. Soc.* **2002**, *124*, 6506–6507. (d) Zhan, W.; Alvarez, J.; Crooks, R. M. *J. Am. Chem. Soc.* **2002**, *124*, 13265–13270.

- (5) (a) Wasielewski, M. R. *Chem. Rev.* **1992**, *92*, 435–461. (b) Balzani, V.; Juris, A.; Venturi, M.; Campagna, S.; Serroni, S. *Chem. Rev.* **1996**, *96*, 759–833. (c) De Cola, L.; Belser, P. *Coord. Chem. Rev.* **1998**, *177*, 301–346. (d) Vlcek, A. *Coord. Chem. Rev.* **2000**, *200*–202, 933–978. (e) Balzani, V.; Juris, A. *Coord. Chem. Rev.* **2001**, *211*, 97–115.
- (6) (a) Baldo, M. A.; O'Brien, D. F.; You, Y.; Shoustikov, A.; Sibley, S.; Thompson, M. E.; Forrest, S. R. *Nature* **1998**, *395*, 151–154. (b) Handy, E. S.; Pal, A. J.; Rubner, M. F. *J. Am. Chem. Soc.* **1999**, *121*, 3525. (c) Gao, F. G.; Bard, A. J. *J. Am. Chem. Soc.* **2000**, *122*, 7426. (d) Lamansky, S.; Djurovich, P.; Murphy, D.; Abdel-Razzaq, F.; Lee, H.-E.; Adachi, C.; Burrows, P. E.; Forrest, S. R.; Thompson, M. E. *J. Am. Chem. Soc.* **2001**, *123*, 4304–4312. (e) Carlson, B.; Phelan, G. D.; Kaminsky, W.; Dalton, L.; Jiang, X.; Liu, S.; Jen, A. K. Y. *J. Am. Chem. Soc.* **2002**, *124*, 14162–14172. (f) Welter, S.; Brunner, K.; Hofstraat, J. W.; De Cola, L. *Nature* **2003**, *421*, 54–57.
- (7) (a) Harriman, A.; Ziessel, R. *Coord. Chem. Rev.* **1998**, *171*, 331–339. (b) Barigelletti, F.; Flamigni, L. *Chem. Soc. Rev.* **2000**, *29*, 1–12.
- (8) (a) Anderson, P. A.; Keene, F. R.; Meyer, T. J.; Moss, J. A.; Strouse, G. F.; Treadway, J. A. *J. Chem. Soc., Dalton Trans.* **2002**, 3820–3831. (b) Molnar, S. M.; Nallas, G.; Bridgewater, J. S.; Brewer, K. J. *J. Am. Chem. Soc.* **1994**, *116*, 5206–5210. (c) Hagfeldt, A.; Grätzel, M. *Acc. Chem. Res.* **2000**, *33*, 269–277.

Table 1. Comparison of the Properties among **0**⁺, **2**⁺, **3**⁺, **1e**⁺, **1h**⁺, and **1j**⁺

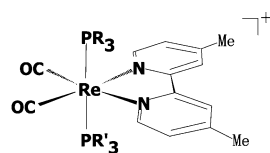
	[Re(X ₂ bpy)(CO) ₂ LL'] ⁺			λ_{abs}^a nm	λ_{em}^b nm	τ_{em}^c ns	$E_{1/2}^{\text{red}}$ V	TN _{CO} ^e
	X	L	L'					
0 ⁺	H	CO	P(OEt) ₃	351	542	1033	−1.59	5.9
2 ⁺	CF ₃	CO	P(OEt) ₃	363	623	162	−1.19	0.1
3 ⁺	H	py	P(OEt) ₃	397	651	12	(−1.64) ^h	~0
1e ⁺	Me	P(<i>p</i> -FPh) ₃	P(<i>p</i> -FPh) ₃	396	595	1046	−1.73	17.3
1h ⁺	Me	PPh ₃	P(OEt) ₃	382	606	511	−1.81	0.5
1j ⁺	Me	P(O- <i>i</i> -Pr) ₃	P(O- <i>i</i> -Pr) ₃	366	605	381	−1.86	0.2

^a ¹MLCT absorption maximum measured in MeCN. ^b Emission maximum measured in MeCN. ^c Lifetime of emission measured in MeCN. ^d Redox potential (X₂bpy/X₂bpy^{•−}) vs Ag/AgNO₃. See General Procedures in Experimental Section. ^e Turnover number of CO formation by reduction of CO₂ using the rhenium complex as photocatalyst. See Photocatalytic Reaction in Experimental Section. ^f Reference 19. ^g Reference 12. ^h Peak potential for the irreversible process.

Two methods are available for changing the properties of these complexes: (i) use of a ligand with a different ligand-field strength, to adjust the energy levels of the d π orbitals in the central metal and (ii) introduction of functional groups with different electro-donating or -accepting properties to the diimine ligand, to adjust the π^* orbital energy level, (these orbitals are related to useful photochemical, photophysical, and electrochemical events).

As typical examples, rhenium diimine complexes, which are useful as CO₂-reduction photocatalysts,^{9,10} electroluminescent devices¹¹ and so on, are shown in Table 1. Although the complex *fac*-[Re(bpy)(CO)₃{P(OEt)₃}]⁺ (**0**⁺; bpy = 2,2'-bipyridine) emits strongly with high quantum yield even in solution at room temperature, and can act as an efficient photocatalyst for CO₂ reduction,^{10a} its absorption in the visible region is very limited,¹² so that it must be modified to allow effective use of solar energy. Introduction of either trifluoromethyl groups to the bpy ligands (**2**⁺),^{10b} or a pyridine ligand having a weaker ligand field than that of the P(OEt)₃ ligand (**3**⁺),¹³ red-shifts the ¹MLCT absorption band by 12–46 nm (see Table 1). However, these changes also lessen their photocatalytic activities, because of the shorter lifetimes of the ³MLCT excited state, which must be quenched by a reductant, and weaker reduction power of the corresponding reduced complex as an important intermediate.¹³ How can the conflicting effects of these perturbations on the properties of metal complexes be canceled and controlled?

We report here a new way to manipulate the properties of metal diimine complexes using intramolecular interactions between ligands, which red-shift the ¹MLCT absorption but

Chart 1^a


Complex	PR ₃	PR' ₃	Σχ ^f
1a ⁺	P(<i>p</i> -MeOPh) ₃	P(<i>p</i> -MeOPh) ₃	21.0
1b ⁺	P(<i>p</i> -MeOPh) ₃	PPh ₃	23.8
1c ⁺	PPh ₃	PPh ₃	26.5
1d ⁺	PPh ₃	P(<i>p</i> -FPh) ₃	29.0
1e ⁺	P(<i>p</i> -FPh) ₃	P(<i>p</i> -FPh) ₃	31.4
1f ⁺	P(<i>p</i> -ClPh) ₃	P(<i>p</i> -ClPh) ₃	33.6
1g ⁺	P(<i>p</i> -MeOPh) ₃	P(O- <i>i</i> -Pr) ₃	29.6
1h ⁺	PPh ₃	P(OEt) ₃	34.9
1i ⁺	P(<i>p</i> -FPh) ₃	P(OMe) ₃	39.8
1j ⁺	P(O- <i>i</i> -Pr) ₃	P(O- <i>i</i> -Pr) ₃	38.1
1k ⁺	P(OEt) ₃	P(OEt) ₃	43.2
1l ⁺	P(OEt) ₃	P(OMe) ₃	45.7

^a Sum of Tolman's χ values of each phosphorus ligand (from ref 23). The χ represents electron-attracting ability of the phosphorus ligand.

blue-shift the emission from ³MLCT, increase the lifetime of the ³MLCT excited state, and provide stronger oxidation power in both the ground state and excited states, stronger reduction power of the one-electron-reduced (OER) complex, and high photocatalytic activity for CO₂ reduction. A series of rhenium-(I) biscarbonyl complexes with two phosphorus ligands at the cis-positions to the 4,4'-dimethyl-2,2'-bipyridine(dmb) ligand (shown in Chart 1) were synthesized: both phosphorus ligands may have π – π and/or CH– π interaction(s) with the dmb ligand.

Experimental Section

General Procedures. IR spectra were recorded with a JEOL JIR-6500 FTIR spectrophotometer using 1 cm^{−1} resolution. UV/vis spectra were measured with a JASCO V-565 or Photol MCPD-2000 spectrophotometer. Emission spectra were recorded at 25 °C using a JASCO FP-6600 spectrofluorometer with correction for the detector sensitivity determined using correction data supplied by JASCO. Emission quantum yields were evaluated with quinine bisulfate ($\Phi_{\text{em}} = 0.546$)¹⁴ as a standard. Emission lifetimes were measured either with a Horiba NAES-1100 time-correlated single-photon-counting system (the excitation source was a nanosecond H₂ lamp, NFL-111, and the instrumental response time was less than 1 ns) or with a Continuum YG680-10 Nd:YAG pulse laser source (third-harmonic generation at 355 nm, 10 ns fwhm, 10 mJ/pulse) and Hamamatsu Photonics R926 photomultiplier tube on a Jobin-Yvon HR-320 monochromator.¹⁵ Proton-NMR spectra were measured in an acetone-*d*₆ solution using a Bruker AC300P (300 MHz) system. Residual protons of acetone-*d*₆ were used as an internal standard for the measurements. Cyclic voltammograms of the complexes were measured in an acetonitrile solution containing tetra-*n*-butylam-

- (9) Hawecker, J.; Lehn, J. M.; Ziessel, R. *Helv. Chim. Acta* **1986**, *69*, 1990–2012.
 (10) (a) Hori, H.; Johnson, F. P. A.; Koike, K.; Ishitani, O.; Ibusuki, T. *J. Photochem. Photobiol. A: Chem.* **1996**, *96*, 171–174. (b) Koike, K.; Hori, H.; Ishizuka, M.; Westwell, J. R.; Takeuchi, K.; Ibusuki, T.; Enjouji, K.; Konno, H.; Sakamoto, K.; Ishitani, O. *Organometallics* **1997**, *16*, 5724–5729. (c) Hori, H.; Johnson, F. P. A.; Koike, K.; Takeuchi, K.; Ibusuki, T.; Ishitani, O. *J. Chem. Soc., Dalton Trans.* **1997**, 1019–1023.
 (11) (a) Lundin, N. J.; Walsh, P. J.; Howell, S. L.; McGarvey, J. J.; Blackman, A. G.; Gordon, K. C. *Inorg. Chem.* **2005**, *44*, 3551–3560. (b) Yam, V. W.-W.; Li, B.; Yang, Y.; Chu, B. W.-K.; Wong, K. M.-C.; Cheung, K.-K. *Eur. J. Inorg. Chem.* **2003**, 4035–4042. (c) Ng, P. K.; Gong, X.; Chan, S. K.; Lam, L. S. M.; Chan, W. K. *Chem.–Eur. J.* **2001**, *7*, 4358–4367. (d) Li, F.; Zhang, M.; Cheng, G.; Feng, J.; Zhao, Y.; Ma, Y.; Liu, S.; Shen, J. *Appl. Phys. Lett.* **2004**, *84*, 148–150. (e) Li, F.; Zhang, M.; Feng, J.; Cheng, G.; Wu, Z.; Ma, Y.; Liu, S.; Sheng, J.; Lee, S. T. *Appl. Phys. Lett.* **2003**, *83*, 365–367.
 (12) Hori, H.; Koike, K.; Ishizuka, M.; Takeuchi, K.; Ibusuki, T.; Ishitani, O. *J. Organomet. Chem.* **1997**, *530*, 169–176.
 (13) Koike, K.; Tanabe, J.; Toyama, S.; Tsubaki, H.; Sakamoto, K.; Westwell, J. R.; Johnson, F. P. A.; Hori, H.; Saitoh, H.; Ishitani, O. *Inorg. Chem.* **2000**, *39*, 2777–2783.

- (14) Melhuish, W. H. *J. Phys. Chem.* **1961**, *65*, 229.
 (15) (a) Koike, K.; Okoshi, N.; Hori, H.; Takeuchi, K.; Ishitani, O.; Tsubaki, H.; Clark, I. P.; George, M. W.; Johnson, F. P. A.; Turner, J. J. *J. Am. Chem. Soc.* **2002**, *124*, 11448–11455. (b) Gholamkhash, B.; Koike, K.; Negishi, N.; Hori, H.; Sano, T.; Takeuchi, K. *Inorg. Chem.* **2003**, *42*, 2919–2932.

monium tetrafluoroborate (0.1 M) as supporting electrolyte using an ALS/CHI620 electrochemical analyzer with a glassy-carbon disk working electrode (3 mm diameter), a Ag/AgNO₃ (0.1 M) reference electrode, and a Pt counter electrode. The supporting electrolyte was dried in vacuo at 100 °C for 1 day prior to use.

Materials. Dimethylformamide (DMF) and triethanolamine (TEOA) were distilled under a reduced pressure from 4 Å molecular sieves and KOH, respectively. Acetonitrile was dried three times over P₂O₅ and then distilled from CaH₂ prior to use. Tetra-*n*-butylammonium tetrafluoroborate was triply recrystallized from ethyl acetate/benzene. Other reagents and solvents were purchased from Kanto Chemical Co., Junsei Chemical Co., Tokyo Kasei Co., Wako Pure Chemical Industries, and Aldrich Chemical Co. and used without further purification.

Synthesis Procedures. The CF₃SO₃[−] and PF₆[−] salts of *fac*-[Re(dmb)(CO)₃(PR₃)₃]⁺ (R = *p*-MeOPh, Ph, *p*-FPh, *p*-ClPh, *O*-*i*-Pr, OEt) and the PF₆[−] salts of *cis,trans*-[Re(dmb)(CO)₂(PPh₃)₂]⁺ (**1c**⁺), *cis,trans*-[Re(dmb)(CO)₂{P(*p*-FPh)₃}₂]⁺ (**1e**⁺), *cis,trans*-[Re(dmb)(CO)₂(PPh₃)-{P(OEt)₃}]⁺ (**1h**⁺), *cis,trans*-[Re(dmb)(CO)₂{P(*O*-*i*-Pr)₃}₂]⁺ (**1j**⁺), and *cis,trans*-[Re(dmb)(CO)₂{P(OEt)₃}₂]⁺ (**1k**⁺) were synthesized according to previously reported methods.^{12,13,15a} Similar methods were used for the synthesis of the following complexes. The reaction solutions were cooled with water during irradiation in all cases.

***cis,trans*-[Re(dmb)(CO)₂{P(*p*-MeOPh)₃}₂]⁺PF₆[−] (**1a**⁺PF₆[−]).** A THF solution (280 mL) containing 106 mg (0.11 mmol) of *fac*-[Re(dmb)(CO)₃{P(*p*-MeOPh)₃}]⁺CF₃SO₃[−] and 455 mg (1.30 mmol) of tris(4-methoxyphenyl)phosphine was irradiated under an argon atmosphere using a high-pressure mercury lamp with an uranyl glass filter (>330 nm) for 1 h. After irradiation the solvent was evaporated under reduced pressure, and the residual orange solid was washed with ether and recrystallized from CH₂Cl₂-ether. To a 2 mL methanolic solution of this solid, a concentrated NH₄⁺PF₆[−] methanolic solution was added dropwise. The precipitated PF₆[−] salts of **1a**⁺ were collected by filtration, washed with water, and then dried in vacuo.

Yield: 69%. Anal. Calcd for C₅₆H₅₄N₂O₈F₆P₃Re: C, 52.71; H, 4.27; N, 2.20. Found: C, 52.64; H, 4.80; N, 2.05. ¹H NMR (δ, 300 MHz, CD₃COCD₃): 8.16 (s, 2H, *bpy*-3,3'), 7.93 (d, 2H, *J* = 5.8 Hz, *bpy*-6,6'), 6.89 (d, 2H, *J* = 5.8 Hz, *bpy*-5,5'), 7.00–7.25 (m, 12H, *Ph*-m), 6.66–6.90 (m, 12H, *Ph*-o), 3.79 (s, 18H, *CH*₃-*O*-Ph), 2.45 (s, 6H, *CH*₃-*bpy*). FT-IR (CH₃CN): ν_{CO}/cm^{−1} = 1930, 1859. UV/vis (CH₃CN): λ_{max}/nm (ε/10³ M^{−1} cm^{−1}) = 415 (2.6), 291 (sh), 273 (sh), 244 (71).

***cis,trans*-[Re(dmb)(CO)₂{P(*p*-MeOPh)₃}₂(PPh₃)]⁺PF₆[−] (**1b**⁺PF₆[−]).** was obtained by irradiation of a THF solution (200 mL) containing 85 mg (0.098 mmol) of *fac*-[Re(dmb)(CO)₃(PPh₃)]⁺CF₃SO₃[−] and 151 mg (0.43 mmol) of tris(4-methoxyphenyl)phosphine under an argon atmosphere for 3 h. After evaporation of the solution, the residue was purified with column chromatography on silica gel using CH₂Cl₂ as eluent. The yellow layer was collected and evaporated under reduced pressure to give the CF₃SO₃[−] salts of **1b**⁺ as a yellow solid, which were recrystallized using ether-CH₂Cl₂. The PF₆[−] salts of **1b**⁺ were obtained using a procedure analogous to that given for **1a**⁺. Elemental analysis data were obtained using the CF₃SO₃[−] salts of **1b**⁺.

Yield: 38%. Anal. Calcd for C₅₂H₄₈N₂O₆F₃P₂ReS: C, 55.07; H, 4.27; N, 2.47. Found: C, 54.81; H, 4.51; N, 2.37. ¹H NMR (δ, 300 MHz, CD₃COCD₃): 8.18 (s, 2H, *bpy*-3,3'), 7.91 (d, 2H, *J* = 5.9 Hz, *bpy*-6,6'), 6.86 (d, 2H, *J* = 5.9 Hz, *bpy*-5,5'), 7.25–7.40 (m, 15H, *Ph*), 7.10–7.25 (m, 6H, *p*-MeOPh), 6.75–6.90 (m, 6H, *p*-MeOPh), 3.79 (s, 9H, *CH*₃-*O*-Ph), 2.44 (s, 6H, *CH*₃-*bpy*). FT-IR (CH₃CN): ν_{CO}/cm^{−1} = 1933, 1861. UV/vis (CH₃CN): λ_{max}/nm (ε/10³ M^{−1} cm^{−1}) = 411 (2.4), 292 (sh), 271 (sh), 238 (44).

***cis,trans*-[Re(dmb)(CO)₂(PPh₃)₂]{P(*p*-FPh)₃}⁺PF₆[−] (**1d**⁺PF₆[−]).** was obtained by irradiation of a THF solution (250 mL) containing 80 mg (0.087 mmol) of *fac*-[Re(dmb)(CO)₃{P(*p*-FPh)₃}]⁺CF₃SO₃[−] and 115 mg (0.44 mmol) of triphenylphosphine under an argon atmosphere for 2 h. After evaporation of the solution, the residue was purified with column chromatography on silica gel using CH₂Cl₂ as eluent. The orange layer was collected and evaporated under reduced pressure to

give the CF₃SO₃[−] salts of **1d**⁺ as a yellow solid, which was recrystallized using ether-CH₂Cl₂. The PF₆[−] salts of **1d**⁺ were obtained in a manner similar to that for **1a**⁺.

Yield: 83%. Anal. Calcd for C₅₀H₃₉N₂O₂F₉P₃Re: C, 52.22; H, 3.42; N, 2.44. Found: C, 52.18; H, 3.31; N, 2.38. ¹H NMR (δ, 300 MHz, CD₃COCD₃): 8.22 (s, 2H, *bpy*-3,3'), 7.94 (d, 2H, *J* = 5.4 Hz, *bpy*-6,6'), 6.91 (d, 2H, *J* = 5.4 Hz, *bpy*-5,5'), 7.20–7.40 (m, 21H, *Ph*, *p*-FPh), 7.00–7.20 (m, 6H, *p*-FPh), 2.45 (s, 6H, *CH*₃-*bpy*). FT-IR (CH₃CN): ν_{CO}/cm^{−1} = 1937, 1867. UV/vis (CH₃CN): λ_{max}/nm (ε/10³ M^{−1} cm^{−1}) = 400 (2.7), 313 (sh), 293 (17), 275 (17), 223 (2h).

***cis,trans*-[Re(dmb)(CO)₂{P(*p*-ClPh)₃}₂]⁺PF₆[−] (**1f**⁺PF₆[−]).** was synthesized in a manner similar to that for the synthesis of **1d**⁺PF₆[−].

Yield: 79%. Anal. Calcd for C₅₀H₃₆N₂O₂Cl₂F₆P₃Re: C, 46.10; H, 2.79; N, 2.15. Found: C, 46.33; H, 2.90; N, 2.12. ¹H NMR (δ, 300 MHz, CD₃COCD₃): 8.23 (s, 2H, *bpy*-3,3'), 8.07 (d, 2H, *J* = 5.6 Hz, *bpy*-6,6'), 7.03 (d, 2H, *J* = 5.6 Hz, *bpy*-5,5'), 7.25–7.45 (m, 24H, *p*-ClPh), 2.49 (s, 6H, *CH*₃-*bpy*). FT-IR (CH₃CN): ν_{CO}/cm^{−1} = 1942, 1872. UV/vis (CH₃CN): λ_{max}/nm (ε/10³ M^{−1} cm^{−1}) = 395 (2.6), 315 (sh), 296 (19), 273 (19), 224 (sh), 232 (22).

***cis,trans*-[Re(dmb)(CO)₂{P(*p*-MeOPh)₃}₂{P(*O*-*i*-Pr)₃}]⁺PF₆[−] (**1g**⁺PF₆[−]).** A THF solution (30 mL) containing 105 mg (0.17 mmol) of *fac*-[Re(dmb)(CO)₃(CF₃SO₃)]⁺ and 1 mL of triisopropyl phosphite was refluxed for 24 h under an argon atmosphere, and then 183 mg (0.52 mmol) of tris(4-methoxyphenyl)phosphine was introduced into the solution. This solution was irradiated for 1 h under an argon atmosphere. The light exposed solution was evaporated and then chromatographed on silica gel using CH₂Cl₂ as eluent. The yellow layer was collected and evaporated under reduced pressure to give the CF₃SO₃[−] salts of **1g**⁺ as a yellow solid, which was recrystallized using ether-CH₂Cl₂. The PF₆[−] salt of **1g**⁺ was obtained in a manner similar to that for **1a**⁺.

Yield: 45%. Anal. Calcd for C₄₄H₅₄N₂O₈F₆P₃Re: C, 46.68; H, 4.81; N, 2.48. Found: C, 46.89; H, 4.79; N, 2.45. ¹H NMR (δ, 300 MHz, CD₃COCD₃): 8.48 (d, 2H, *J* = 5.9 Hz, *bpy*-6,6'), 8.37 (s, 2H, *bpy*-3,3'), 7.33 (d, 2H, *J* = 5.9 Hz, *bpy*-5,5'), 7.13–7.23 (m, 6H, *p*-MeOPh), 6.82–6.89 (m, 6H, *p*-MeOPh), 4.50–4.67 (m, 3H, POCH(CH₃)₂), 3.81 (s, 9H, *CH*₃-*O*-Ph), 2.55 (s, 6H, *CH*₃-*bpy*), 1.03 (d, 18H, *J* = 5.9 Hz, POCH(CH₃)₂). FT-IR (CH₃CN): ν_{CO}/cm^{−1} = 1939, 1865. UV/vis (CH₃CN): λ_{max}/nm (ε/10³ M^{−1} cm^{−1}) = 388 (3.3), 312 (sh), 285 (sh), 246 (41).

***cis,trans*-[Re(dmb)(CO)₂{P(*p*-FPh)₃}₂{P(OMe)₃}]⁺PF₆[−] (**1i**⁺PF₆[−]).** The acetonitrile complex *cis,trans*-[Re(dmb)(CO)₂(MeCN){P(*p*-FPh)₃}]⁺PF₆[−] was synthesized by irradiation to an acetonitrile solution (250 mL) containing 180 mg (0.203 mmol) of *fac*-[Re(dmb)(CO)₃{P(*p*-FPh)₃}]⁺PF₆[−] under an argon atmosphere for 1 h, and then the solvent was evaporated under reduced pressure. The resulting yellow solid was dissolved into 50 mL of a THF solution containing 1 mL of trimethyl phosphite and refluxed for 36 h under an argon atmosphere. After evaporation of the solution, the residue was purified with column chromatography on silica gel using CH₂Cl₂ as eluent. The orange layer was collected and evaporated under reduced pressure to give **1i**⁺PF₆[−] as yellow solid, which was recrystallized using ether-CH₂Cl₂.

Yield: 20%. Anal. Calcd for C₃₅H₃₃N₂O₅F₉P₃Re: C, 41.55; H, 3.29; N, 2.77. Found: C, 41.98; H, 3.26; N, 2.85. ¹H NMR (δ, 300 MHz, CD₃COCD₃): 8.54 (d, 2H, *J* = 5.9 Hz, *bpy*-6,6'), 8.44 (s, 2H, *bpy*-3,3'), 7.27–7.38 (m, 2H, *bpy*-5,5'), 7.27–7.38 (m, 6H, *p*-FPh), 7.11–7.18 (m, 6H, *p*-FPh), 3.50 (d, 9H, *J*_{H,P} = 11.0 Hz, POCH₃), 2.55 (s, 6H, *CH*₃-*bpy*). FT-IR (CH₃CN): ν_{CO}/cm^{−1} = 1950, 1877. UV/vis (CH₃CN): λ_{max}/nm (ε/10³ M^{−1} cm^{−1}) = 379 (3.8), 311 (sh), 287 (18), 267 (20), 257 (sh), 232 (26).

***cis,trans*-[Re(dmb)(CO)₂{P(OEt)₃}₂{P(OMe)₃}]⁺PF₆[−] (**1l**⁺PF₆[−]).** was obtained by irradiation to a THF solution (90 mL) containing 50 mg (0.065 mmol) of *fac*-[Re(dmb)(CO)₃{P(OMe)₃}]⁺PF₆[−] and 2 mL of triethylphosphite under an argon atmosphere for 1 h. After evaporation of the solution, the residual yellow solid was washed with ether and then recrystallized from CH₂Cl₂-ether.

Table 2. Crystallographic Data for $1e^+CF_3SO_3^-$

empirical formula	$C_{51}H_{36}F_9N_2O_3P_2ReS$
formula weight	1208.0
crystal system	triclinic
space group	$P\bar{1}$
$a/\text{\AA}$	15.5782(16)
$b/\text{\AA}$	13.5247(11)
$c/\text{\AA}$	13.0531(9)
α/deg	116.249(3)
β/deg	79.374(6)
γ/deg	95.966(4)
$V/\text{\AA}^3$	2423.5(4)
Z	2
T/K	253
R_{int}	0.0435
number of total reflections	23 566
number of parameters	642
$R1[I > 2\sigma(I)]^a$	0.0339
$wR2[I > 2\sigma(I)]^b$	0.0824
GOF ^c on F^2	1.066

^a $R1 = \sum(|F_o| - |F_c|)/\sum|F_o|$. ^b $wR2 = [\sum[w(F_o^2 - F_c^2)^2]/\sum[w(F_o^2)]^{1/2}$.
^c GOF = $[\sum w(|F_o|^2 - |F_c|^2)^2/(m - n)]^{1/2}$, where m = number of reflections and n = number of parameters.

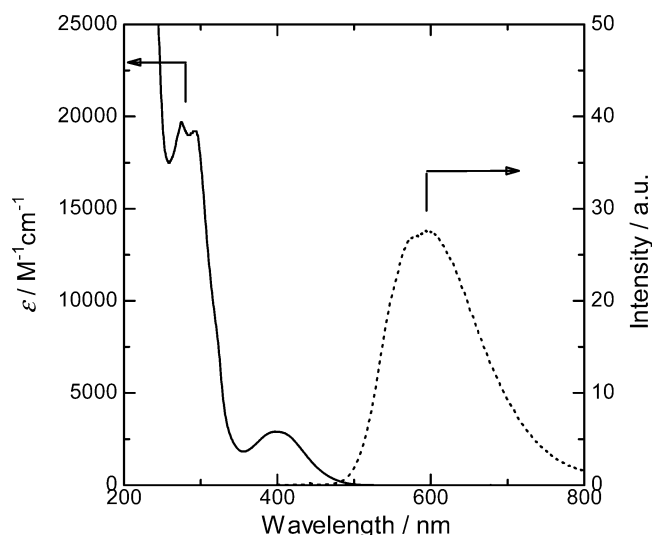
Yield: 87%. Anal. Calcd for $C_{23}H_{36}N_2O_8F_6P_3Re$: C, 32.06; H, 4.21; N, 3.25. Found: C, 32.53; H, 4.11; N, 3.18. 1H NMR (δ , 300 MHz, CD_3COCD_3): 8.92 (d, 2H, $J = 5.9$ Hz, bpy -6,6'), 8.59 (s, 2H, bpy -3,3'), 7.62 (d, 2H, $J = 5.9$ Hz, bpy -5,5'), 3.86 (dq, 6H, $J_{HH} = J_{HP} = 7.0$ Hz, $POCH_2CH_3$), 3.48 (dd, 9H, $J_{HP} = 10.3$, 0.7 Hz, $POCH_3$), 2.63 (s, 6H, CH_3 - bpy), 1.02 (t, 9H, $J = 7.0$ Hz, $POCH_2CH_3$). FT-IR (CH_3CN): $\nu_{CO}/\text{cm}^{-1} = 1956, 1882$. UV/vis (CH_3CN): $\lambda_{\text{max}}/\text{nm}$ ($\epsilon/10^3 \text{ M}^{-1} \text{ cm}^{-1}$) = 363 (4.2), 309 (sh), 281 (16), 264 (18), 256 (17).

Crystal Structure Determination. The single crystals of $1e^+CF_3SO_3^-$ were obtained by slow diffusion of diethyl ether into a dichloromethane solution containing the complex. Diffraction data of $1e^+CF_3SO_3^-$ were collected on a Rigaku RAPID imaging-plate diffractometer with graphite-monochromated Mo $K\alpha$ radiation ($\lambda = 0.71073 \text{ \AA}$) using yellow needle crystals, $0.4 \times 0.1 \times 0.1 \text{ mm}^3$ at 253 K with a Rigaku low-temperature apparatus (-20°C). The intensity data were corrected for Lorentz and polarization effects. The structure was solved by the direct methods using the TEXSAN program¹⁶ and was refined on F^2 by means of full-matrix least-squares procedures, using the SHELXL-97 program.¹⁷ No secondary extinction corrections were applied. In the least-squares refinements, all non-hydrogen atoms were refined with anisotropic displacement parameters, but all hydrogen atoms were refined using the riding model isotropic thermal parameters which are 1.2 times those of the attached carbon atoms. Details of the crystallographic data are given in Table 2.

Quenching Experiments. Reductive-quenching experiments of the excited complexes were carried out using TEOA as an electron donor. At least four samples for each complex were prepared as DMF solutions, with various TEOA concentrations between 0 and 0.6 M. Stern–Volmer plots of the observed decrease in emission intensity with increasing of TEOA concentration showed a good linear relation with an intercept of 1, so that the reductive-quenching rate constant k_q can be calculated using eq 1 and the emission lifetime of the complex in the absence of TEOA τ_{em} .

$$I_0/I = 1 + k_q\tau_{em}[\text{TEOA}] \quad (1)$$

Photocatalytic Reaction. A 4 mL aliquot of DMF–TEOA (5:1 v/v) solution containing each of the rhenium complexes (0.5 mM) was introduced into a quartz cell (7 mL volume), and CO_2 was bubbled through for 20 min before the cell was sealed using a rubber septum (Aldrich). The sample solution was kept at $25 \pm 1^\circ\text{C}$ and was irradiated

**Figure 1.** UV/vis absorption (solid line) and emission spectra (dotted line) of $1e^+$ measured in acetonitrile solution at 298 K.

at 365 nm using a 500 W high-pressure mercury lamp with both band-pass and ND filters (Asahi Bunko Co.). A gas sample was taken using a gastight syringe, and the reaction products, i.e., CO and H_2 , were measured using a Shimadzu GC-9A gas chromatograph with a TCD detector. The light intensity incident into the cell was 8.22×10^{-9} einstein s^{-1} for $1a^+$, $1c^+$, $1e^+$, $1f^+$, $1h^+$, and $1j^+$, and 5.24×10^{-9} einstein s^{-1} for $1b^+$, $1d^+$, $1g^+$, $1i^+$, $1k^+$, and $1l^+$, determined using a $K_3Fe(C_2O_4)_3$ actinometer.

Results

UV/vis Absorption, Emission, and IR Spectra. Figure 1 shows typical UV/vis absorption and emission spectra of $1e^+$.

A metal-to-ligand (dmb) charge transfer (MLCT) absorption band was observed with an absorption maximum at 396 nm; the intense and relatively sharp band around 292 nm is attributable to dmb-localized $\pi-\pi^*$ absorption.^{13,18a} All complexes strongly emit from their 3MLCT excited states in acetonitrile solution at room temperature, and these emission bands were unstructured and broad, similar to those in Figure 1. Table 3 summarizes the absorption and emission maxima, the apparent stokes shifts ($\Delta E_{\text{abs-em}}$), the molar extinction coefficients, the emission lifetimes (τ_{em}), and the emission quantum yields (Φ_{em}) with radiative and nonradiative decay rate constants k_r and k_{nr} calculated using the following equations, since all complexes investigated in this work were stable against irradiation at 400 nm.

$$k_r = \Phi_{em}/\tau_{em} \quad (6)$$

$$k_{nr} = (1 - \Phi_{em})/\tau_{em} \quad (7)$$

In IR spectra of all the complexes we observed two CO stretching bands, attributable to symmetric and antisymmetric vibrations in *cis*-biscarbonyl rhenium bipyridine complexes with a C_{2v} symmetry.¹³ In these cases, the principal force constant k_{CO} and the interaction force constant $k_{CO,CO}$ both can be calculated using energy factored force field (EFFF) theory.¹⁸ The results are summarized in Table 4.

(16) Corporation, M. S. TEXSAN, Program for the Crystal Structure; The Woodlands, TX 77381-5209, USA, 2000.

(17) Sheldrick, G. M. SHELXL97, Program for the Crystal Structure; University of Göttingen: Germany, 1997.

(18) (a) Ishitani, O.; George, M. W.; Ibusuki, T.; Johnson, F. P. A.; Koike, K.; Nozaki, K.; Pac, C.; Turner, J. J.; Westwell, J. R. *Inorg. Chem.* **1994**, *33*, 4712–4717. (b) Braterman, P. S. *Metal Carbonyl Spectra*; Academic Press: London, 1975.

Table 3. Photophysical Properties of 1^+ Measured in MeCN Solution at 298 K^a

complex	$\lambda_{\text{abs}}(\text{MLCT})$ nm	$\lambda_{\text{abs}}(\pi\text{--}\pi^*)$ nm	λ_{em} nm	$\Delta E_{\text{abs--em}}^b$ cm ^{−1}	τ_{em} ns	Φ_{em}^c	$k_r^d \times 10^4 \text{ s}^{-1}$	$k_{\text{nr}}^e \times 10^4 \text{ s}^{-1}$
1a ⁺	415	291	618	7920	1224	0.07	5.5	76
1b ⁺	411	292	608	7880	1101	0.09	8.2	83
1c ⁺	402	294	600	8210	1074	0.08	7.8	90
1d ⁺	400	293	598	8280	1003	0.07	7.0	93
1e ⁺	396	292	595	8440	1046	0.10	10	93
1f ⁺	395	296	592	8430	1220	0.13	11	71
1g ⁺	388	285	612	9430	601	0.03	5.0	150
1h ⁺	382	288	606	9680	511	0.05	9.8	190
1i ⁺	379	287	602	9780	665	0.06	9.0	140
1j ⁺	366	284	605	10 790	381	0.03	7.9	260
1k ⁺	365	283	603	10 820	355	0.03	8.5	270
1l ⁺	363	281	602	10 940	361	0.05	14	260

^a All complexes are PF₆[−] salts. ^b Apparent Stokes shift defined as $\Delta E_{\text{abs--em}} = E_{\text{abs}} - E_{\text{em}}$. ^c Quantum yield of emission: experimental error was within 10%. ^d Radiative decay rate constant. ^e Nonradiative decay rate constant.

Table 4. ν_{CO} Frequencies and Force Constants for 1^+ and the Corresponding One-Electron-Reduced Species in MeCN Solution at 298 K^a

complex	ν_{CO} cm ^{−1}	k_{CO}^b N m ^{−1}	$k_{\text{CO,CO}}^c$ N m ^{−1}	OER species ^d				
				ν_{CO} cm ^{−1}	k_{CO}^b N m ^{−1}	$k_{\text{CO,CO}}^c$ N m ^{−1}	Δk_{CO}^e N m ^{−1}	$\Delta k_{\text{CO,CO}}^e$ N m ^{−1}
1a ⁺	1930 1859	1451	54.3	1902 1825	1404	58.0	−47	−3.7
1b ⁺	1933 1861	1454	55.2					
1c ⁺	1936 1865	1460	54.5	1908 1830	1412	58.9	−48	−4.4
1d ⁺	1937 1867	1462	53.8					
1e ⁺	1939 1869	1465	53.8	1910 1834	1416	57.5	−49	−3.7
1f ⁺	1942 1872	1470	53.9	1912 1837	1420	56.8	−50	−2.9
1g ⁺	1939 1865	1462	56.9					
1h ⁺	1945 1872	1472	56.3	1917 1840	1426	58.4	−46	−2.1
1i ⁺	1950 1877	1480	56.4					
1j ⁺	1946 1871	1472	57.8	1919 1840	1428	60.0	−44	−2.2
1k ⁺	1953 1879	1484	57.3					
1l ⁺	1956 1882	1488	57.4					

^a All complexes are PF₆[−] salts. ^b Principal force constant. ^c Interaction force constant. ^d The one-electron-reduced species were electrochemically produced in acetonitrile solution containing 0.1 M Et₄NBF₄ under Ar atmosphere. See ref 18a. ^e Differences between the OER species and their parent complexes.

Electrochemical Behavior. Figure 2 shows cyclic voltammograms of **1e**⁺, **1h**⁺, and **1j**⁺ as typical examples. For all complexes, one reversible wave was observed in the cathodic scan, attributable to a dmb-based one-electron reduction. Reversibility of a one-electron oxidation wave attributable to metal-based, e.g., Re^I/Re^{II}, was different; however, a reversible or quasireversible wave was observed for complexes with two trialkylphosphite ligands (**1j**⁺–**1l**⁺), but oxidation waves of complexes with two triarylphosphine ligands (**1a**⁺–**1f**⁺) were irreversible. Table 5 summarizes the electrochemical data.

Crystal Structures. X-ray crystallographic analysis of **1e**⁺CF₃SO₃[−] was performed. Tables 2 and 6 summarize the crystallographic data and selected bond lengths and angles. The

ORTEP drawing of **1e**⁺ is shown in Figure 3 together with that of **1h**⁺, which we have previously reported.¹³ Comparison of the structure of **1e**⁺, with two P(*p*-FPh)₃ ligands, and that of **1h**⁺, with one PPh₃ and one P(OEt)₃ ligand, is interesting, because intramolecular interactions in these complexes are different. The configurations of the atoms around the rhenium metal are very similar in these two complexes except for the Re–P bond lengths. For Re–PPh₃ these are 2.41 Å–2.45 Å in both complexes, whereas Re–P(OEt)₃ in **1h**⁺ was 2.35 Å, similar to Re–P bonds reported for [Re(bpy)(CO)₃(PR₃)]⁺-type complexes.¹⁹

We have previously reported that intramolecular π – π and CH– π interactions exist between the bpy ligand and the aryl groups (Ar) of the PAR₃ ligand in *fac*-[Re(bpy)(CO)₃(PAR₃)]⁺.¹⁹ Similar intramolecular π – π and CH– π interactions were observed in **1h**⁺PF₆[−] and are respectively drawn using red or blue dotted lines in Figure 3b; its pyridine rings were distorted (see Supporting Information); such distortion was also observed in *fac*-[Re(bpy)(CO)₃(PAR₃)]⁺. Two pyridine rings of the dmb ligand are π -stacked with two phenyl groups on the triphenylphosphine. The distances between the centers of π -stacked rings are 3.85 Å and 3.95 Å, and the angles between the rings are 21.53° and 35.02°, respectively.²⁰ The distance between C(7) in the pyridine ring and H(32) in the phenyl group is 2.94 Å, which is less than the sum of the corresponding van der Waals radii.

Intramolecular interactions also exist among the two P(*p*-FPh)₃ ligands and the dmb ligand in crystals of **1e**⁺CF₃SO₃[−]. In this case, each pyridine ring is sandwiched between two aryl groups. One of these aryl groups interacts with the pyridine ring in parallel fashion (red dotted lines in Figure 3a), where the plane–plane distances are 3.55 Å and 4.18 Å and the plane–plane angles are 12.94(22)° and 19.07(32)°, respectively. The second aryl group is closely placed in the pyridine ring with a larger angle, 54.20(19)° and 46.05(19)°, where the distances between H(16) and C(8) and between H(28) and C(3), 2.89 Å and 2.81 Å, both are less than the sums of the corresponding van der Waals radii (blue dotted lines in Figure 3a). Consequently, each of the two pyridine rings interacts with two sets of two phenyl groups; two CH(phenyl)– π (pyridine)– π (phenyl) interactions exist among the dmb ligand and the two P(*p*-XPh)₃ ligands in **1e**⁺CF₃SO₃[−].

¹H NMR Spectra. All complexes displayed three signals due to the dmb-aromatic-ring protons and one singlet due to the methyl groups on the dmb ligand, as summarized in Table 7. The data show that two pyridine rings of the dmb ligand are equivalent; at 25 °C the phosphine ligands can rotate around the Re–P bonds on the NMR time scale. Strong shielding effects by the aryl groups of the phosphine ligand(s) are observed in the dmb-aromatic-ring protons and even in the methyl protons in **1a**⁺–**1i**⁺, especially in **1a**⁺–**1f**⁺, in contrast with **1j**⁺–**1l**⁺ which have no aryl group in the phosphorus ligands. Similar shielding effects have been reported for ruthenium(II)²¹ and rhenium(I)¹⁹ bpy complexes, with π – π interaction between the bpy ligand and a phenyl ring bounded to another ligand. The strong shielding effects observed in **1a**⁺–**1i**⁺ therefore suggest

(19) Tsubaki, H.; Tohyama, S.; Saitoh, H.; Sakamoto, K.; Ishitani, O. *Dalton Trans.* **2005**, 385–395.

(20) Janiak, C. *J. Chem. Soc., Dalton Trans.* **2000**, 3885–3896.

(21) Bolger, J. A.; Ferguson, G.; James, J. P.; Long, C.; McArdle, P.; Vos, J. G. *J. Chem. Soc., Dalton Trans.* **1993**, 1577–1583.

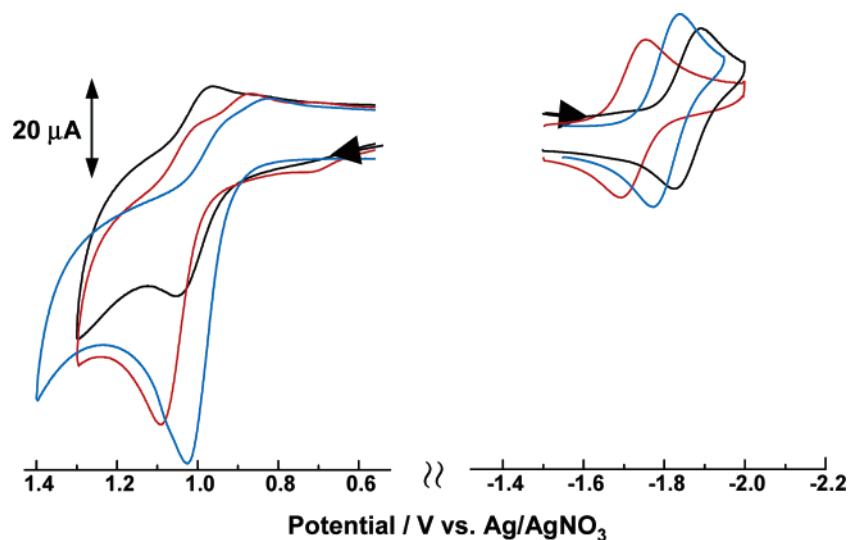


Figure 2. Cyclic voltammograms of $1e^+$ (red) and $1h^+$ (blue) and $1j^+$ (black) measured in acetonitrile solution containing $n\text{-Bu}_4\text{NBF}_4$ (0.1 M) using a glassy carbon working electrode, a Pt counter electrode, and a Ag/AgNO_3 (0.1 M) reference electrode. The scan rate was 200 mV/s.

Table 5. Electrochemical Data for 1^{+a}

complex	E (V vs Ag/AgNO_3)	
	$E_{1/2}^{\text{red } b}$ (dmb/dmb $^{+}$)	$E_p^{\text{ox } c}$ ($\text{Re}/\text{Re}^{\text{II}}$)
$1a^+$	−1.83 (74)	+0.80
$1b^+$	−1.81 (66)	+0.89
$1c^+$	−1.79 (65)	+0.99
$1d^+$	−1.75 (65)	+1.04
$1e^+$	−1.73 (62)	+1.09
$1f^+$	−1.71 (66)	+1.11
$1g^+$	−1.85 (66)	+0.89
$1h^+$	−1.81 (66)	+1.04
$1i^+$	−1.74 (63)	+1.10
$1j^+$	−1.86 (63)	+1.05
$1k^+$	−1.82 (65)	+1.04(81)
$1l^+$	−1.79 (66)	+1.08(85)

^a All complexes are PF_6^- salts. Cyclic voltammograms were taken in MeCN solution containing 0.1 M $n\text{-Bu}_4\text{NBF}_4$ at a 200 mV/s scan rate using a glassy carbon working electrode, a Pt counter electrode, and a 0.1 M Ag/AgNO_3 reference electrode under Ar atmosphere. ^b Redox potential for a reversible or quasireversible wave and peak potential difference in parentheses. ^c Peak potential for irreversible oxidation.

Table 6. Selected Bond Lengths (Å) and Angles (deg) for $1e^+\text{CF}_3\text{SO}_3^-$

Bond Lengths			
$\text{Re}(1)\text{--P}(1)$	2.4135(10)	$\text{Re}(1)\text{--P}(2)$	2.4211(9)
$\text{Re}(1)\text{--N}(1)$	2.182(3)	$\text{Re}(1)\text{--N}(2)$	2.182(3)
$\text{Re}(1)\text{--C}(1)$	1.906(4)	$\text{Re}(1)\text{--C}(2)$	1.903(4)
$\text{C}(1)\text{--O}(1)$	1.158(5)	$\text{C}(2)\text{--O}(2)$	1.153(5)
Bond Angles			
$\text{P}(1)\text{--Re}(1)\text{--N}(1)$	89.99(10)	$\text{P}(1)\text{--Re}(1)\text{--N}(2)$	92.36(9)
$\text{P}(1)\text{--Re}(1)\text{--C}(1)$	87.90(11)	$\text{P}(1)\text{--Re}(1)\text{--C}(2)$	90.15(12)
$\text{P}(2)\text{--Re}(1)\text{--N}(1)$	91.04(10)	$\text{P}(2)\text{--Re}(1)\text{--N}(2)$	89.07(9)
$\text{P}(2)\text{--Re}(1)\text{--C}(1)$	90.78(11)	$\text{P}(2)\text{--Re}(1)\text{--C}(2)$	89.07(12)
$\text{N}(1)\text{--Re}(1)\text{--N}(2)$	74.58(11)	$\text{N}(1)\text{--Re}(1)\text{--C}(1)$	97.65(14)
$\text{N}(1)\text{--Re}(1)\text{--C}(2)$	168.86(14)	$\text{N}(2)\text{--Re}(1)\text{--C}(1)$	172.23(14)
$\text{N}(2)\text{--Re}(1)\text{--C}(2)$	94.28(14)	$\text{C}(1)\text{--Re}(1)\text{--C}(2)$	93.48(16)
$\text{P}(1)\text{--Re}(1)\text{--P}(2)$	178.42(3)		

that the intramolecular interactions between the dmb and the triarylphosphine ligands remain even in solution. This hypothesis is also supported by comparison of the spectroscopic and electrochemical data of $1a^+ \text{--} 1f^+$, $1g^+ \text{--} 1l^+$, and $1j^+ \text{--} 1i^+$; see the Discussion section.

Discussion

Intramolecular Interactions between Ligands. X-ray crystallographic analysis data of $1h^+$ with both the PPh_3 ligand and the $\text{P}(\text{OEt})_3$ ligand (Figure 3b) demonstrate that two sets of intramolecular $\pi\text{--}\pi$ interactions are present between two of the three phenyl groups on the PPh_3 ligand and two pyridine rings in the dmb ligand and that $\text{CH--}\pi$ interaction also takes place between one of the phenyl groups on PPh_3 and the pyridine ring on dmb. Intramolecular interactions were not observed between the triethyl phosphite and the dmb ligands. The crystal structures of nine $\text{fac}[\text{Re}(\text{bpy})(\text{CO})_3(\text{PR}_3)]^+$ -type complexes¹⁹ clearly indicate that, in complexes with a triarylphosphine ligand, similar $\pi\text{--}\pi$ and $\text{CH--}\pi$ interactions exist between the aryl group and the bpy ligand in crystal. Their ^1H NMR and UV-vis spectra and redox potentials strongly suggest that such weak interactions are maintained even in solution, but these weak interactions were not observed in the cases of complexes with a trialkyl- and triphenyl phosphite. On the other hand, the dmb ligand in $1e^+$ is sandwiched between four of the six 4-fluorophenyl groups on the two phosphine ligands, as shown in Figure 3a. The two phenyl groups are parallel to each of the pyridine rings, where $\pi\text{--}\pi$ interactions were observed, and the other two phenyls are sited above each pyridine ring with dihedral angles 54.20° and 46.05°, where $\text{CH--}\pi$ interactions were observed; specifically, two sets of three-centered $\text{CH}(\text{phenyl})\text{--}\pi(\text{pyridine})\text{--}\pi(\text{phenyl})$ interactions operated on both pyridine rings of dmb.

Proton-NMR data obtained in an acetone- d_6 solution (Table 7) show that the chemical shifts for dmb-protons of the complexes with one ($1g^+ \text{--} 1i^+$) and two ($1a^+ \text{--} 1f^+$) triarylphosphine ligand(s) were shifted upfield by 0.2–0.4 ppm and 0.4–1.0 ppm, respectively, compared to complexes with no triarylphosphine ligand ($1j^+ \text{--} 1l^+$). This suggests that the weak interactions observed in crystal remain even in solutions, and the similarities in each group suggest that configurations among the dmb ligand and the phosphorus ligands are similar in each group, so that similar $\text{CH}(\text{phenyl})\text{--}\pi(\text{pyridine})\text{--}\pi(\text{phenyl})$ interactions exist in $1a^+ \text{--} 1d^+$ and $1f^+$, and $\pi\text{--}\pi$ and $\text{CH--}\pi$ interactions exist in $1g^+$ and $1i^+$.

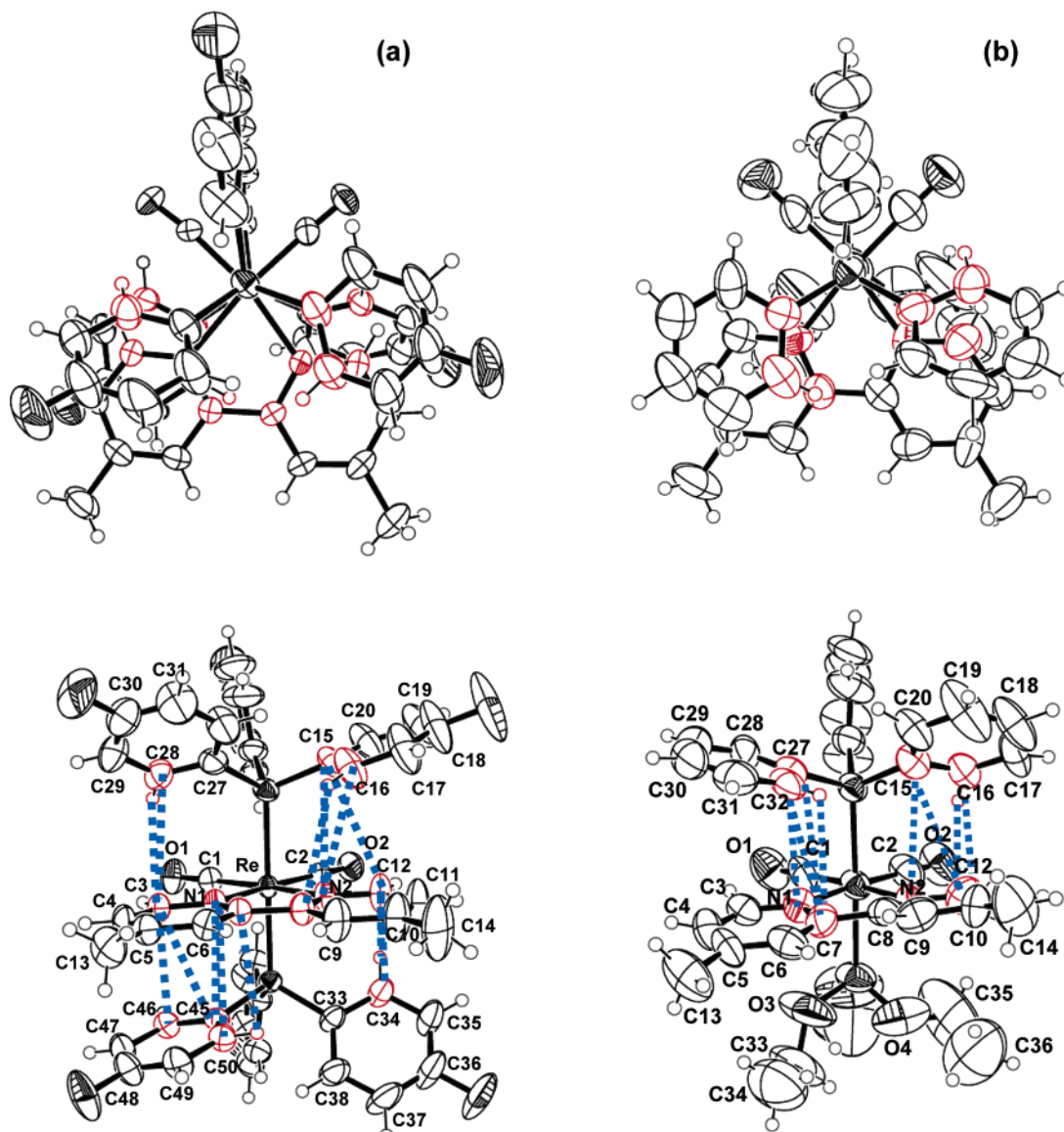


Figure 3. ORTEP drawings of (a) $1e^+CF_3SO_3^-$ and (b) $1h^+PF_6^-$. Displacement ellipsoids are shown at the 50% probability level. Counteranions were omitted for clarity.

Table 7. 1H NMR Chemical Shift Data for the dmb Ligand of 1^+ in Acetone- d_6 Solution^a

complex	$\delta/ppm (J/Hz)$			
	3,3'	5,5'	6,6'	CH ₃
1a ⁺	8.16 (s)	6.89 (d, 5.8)	7.93 (d, 5.8)	2.45 (s)
1b ⁺	8.18 (s)	6.86 (d, 5.9)	7.91 (d, 5.9)	2.44 (s)
1c ⁺	8.12 (s)	6.81 (d, 5.9)	7.87 (d, 5.9)	2.44 (s)
1d ⁺	8.22 (s)	6.91 (d, 5.8)	7.94 (d, 5.5)	2.45 (s)
1e ⁺	8.27 (s)	7.01 (d, 5.9)	8.01 (d, 5.9)	2.47 (s)
1f ⁺	8.23 (s)	7.03 (d, 5.1)	8.07 (d, 5.6)	2.49 (s)
1g ⁺	8.37 (s)	7.33 (d, 5.6)	8.48 (d, 5.9)	2.55 (s)
1h ⁺	8.36 (s)	7.39 (d, 5.5)	8.48 (d, 5.5)	2.54 (s)
1i ⁺	8.44 (s)	7.27–7.38	8.54 (d, 5.9)	2.55 (s)
1j ⁺	8.62 (s)	7.68 (d, 5.9)	8.89 (d, 5.5)	2.64 (s)
1k ⁺	8.60 (s)	7.63 (d, 5.7)	8.91 (d, 5.7)	2.63 (s)
1l ⁺	8.59 (s)	7.62 (d, 5.9)	8.92 (d, 5.9)	2.63 (s)

^a All complexes are PF_6^- salts.

Effects on the Ground State. The principal force constant k_{CO} of the CO ligands is a reliable measure of the electron density on the $d\pi$ orbitals of the central rhenium, since π -back-donation from $d\pi$ orbitals to the antibonding π^* orbital of CO

strongly influences k_{CO} .^{19,22} Figure 4 shows the relation between k_{CO} and the sum of the Tolman χ values of each phosphorus ligand ($\Sigma\chi$); these are used as a measure of the electron accepting ability of a phosphorus ligand.²³ The good linear relation clearly shows that the electron densities on the $d\pi$ orbitals of the central rhenium are affected by the phosphorus ligands through the P–Re bonds. Almost no effect of the intramolecular through-space interactions between ligands is observed.

The dmb-based reduction potential $E_{1/2}(dmb/dmb^{\bullet-})$ is strongly affected by the intramolecular interactions between the dmb and triarylphosphine ligands. As shown in Figure 5, three lines can be drawn for the relation between $E_{1/2}(dmb/dmb^{\bullet-})$ and $\Sigma\chi$, depending on the number of triarylphosphine ligands: **1a**⁺–**1f**⁺ with two triarylphosphine ligands; **1g**⁺–**1i**⁺ with one triarylphosphine ligand; **1j**⁺–**1l**⁺ with no triarylphosphine ligands. If the phosphorus ligands affect the electron accepting

(22) The oxidation potential $E_{p,a}(Re^I/Re^{II})$ cannot be used as a reliable measure of the electron density on $d\pi$ orbitals of the central rhenium because of the considerable difference in reversibility of the oxidation wave on the cyclic voltammograms, as seen in Figure 2.

(23) Tolman, C. A. *Chem. Rev.* **1977**, 77, 313–348.

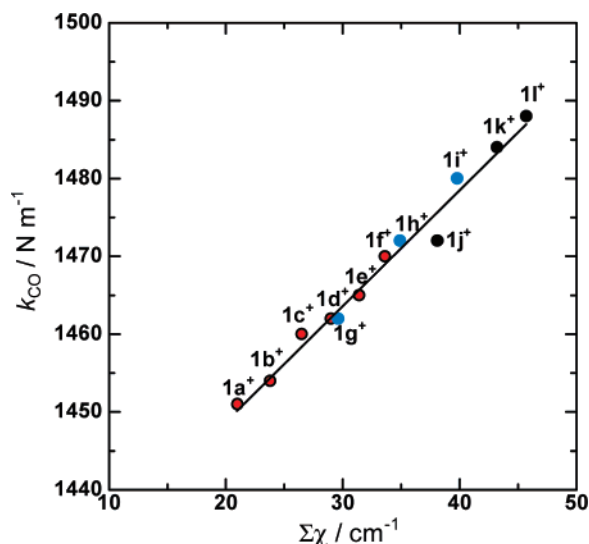


Figure 4. Plots of k_{CO} against $\Sigma\chi$ values of the PR_3 ligands.

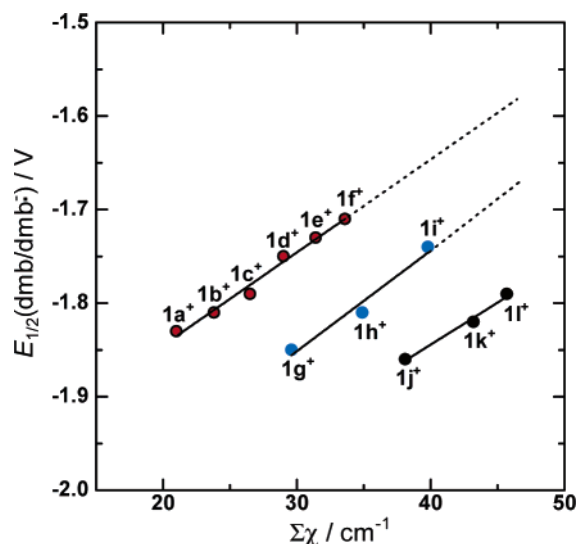


Figure 5. Variations of $E_{1/2}$ (dmb/dmb $^{+}$) with $\Sigma\chi$ values of the PR_3 ligands (in acetonitrile solution containing 0.1 M $n\text{-Bu}_4\text{NBF}_4$; potentials are vs a Ag/AgNO $_3$ reference electrode).

ability of the dmb ligand mostly through the P–Re–N bonds, so that there is no effect of the intramolecular interactions between the dmb and phosphorus ligands, only one straight line would exist in Figure 5. In each of the three groups of the complexes, a good linear relation was observed between $\Sigma\chi$ and $E_{1/2}(\text{dmb}/\text{dmb}^{+})$. It follows that the effect of the intramolecular through-space interactions between ligands can be distinguished from the effect of the N–Re–P through-bond interactions. By extrapolating the lines, we deduce that the intramolecular π – π and CH– π interactions shift $E_{1/2}(\text{dmb}/\text{dmb}^{+})$ positively by ca. 110 mV and the CH(phenyl)– π (pyridine)– π (phenyl) interactions by 180–200 mV.

The intramolecular interactions also affect the UV/vis absorption spectra of the complexes. Figure 6 illustrates the relation between the absorption maximum of the MLCT band and $\Sigma\chi$, where there are again three lines depending on the number of triarylphosphine ligands. Differences between $\mathbf{1g}^{+}$ – $\mathbf{1i}^{+}$ with one triarylphosphine ligand and $\mathbf{1j}^{+}$ – $\mathbf{1l}^{+}$ with no triarylphosphine ligands were 11–19 nm (100–160 meV) and between $\mathbf{1a}^{+}$ – $\mathbf{1f}^{+}$ with two triarylphosphine ligands and $\mathbf{1j}^{+}$ – $\mathbf{1l}^{+}$ were

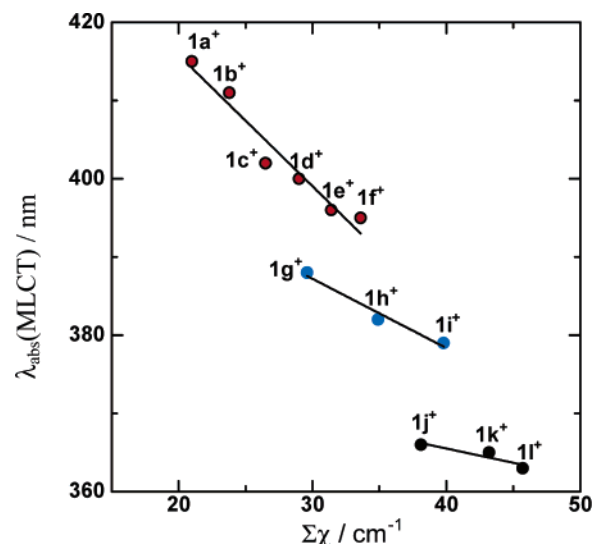


Figure 6. Variations of MLCT absorption maxima $\lambda_{\text{abs}}(\text{MLCT})$ (in acetonitrile solution at 298 K) with $\Sigma\chi$ values of the PR_3 ligands.

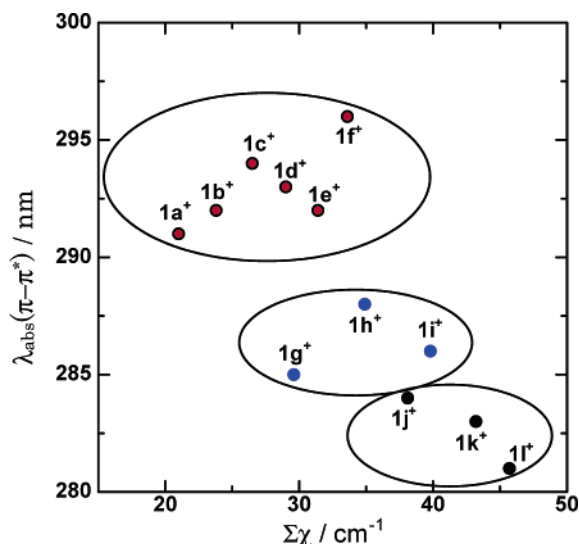


Figure 7. Variations of π – π^* (dmb) absorption maxima $\lambda_{\text{abs}}(\pi$ – $\pi^*)$ (in acetonitrile solution at 298 K) with $\Sigma\chi$ values of the PR_3 ligands.

10–43 nm (110–340 meV), in good agreement with the differences in $E_{1/2}(\text{dmb}/\text{dmb}^{+})$ described above. This is reasonable because the energy of MLCT absorption is proportional to the difference in energy levels between the π^* orbital of the dmb ligand and the $d\pi$ orbital of the central rhenium.

Another band attributed to dmb-ligand centered π – π^* absorption was also red-shifted by the intramolecular interactions. The energy of the absorption was only weakly affected by $\Sigma\chi$ of the phosphorus ligands, probably because the energy of the π orbital is also shifted by the P–Re–N through-bond interaction, with the same direction of the energy shift of the π^* orbital; the average differences from $\mathbf{1j}^{+}$ – $\mathbf{1l}^{+}$ with no triarylphosphine ligands were 1–7 nm (20–110 meV) for $\mathbf{1g}^{+}$ – $\mathbf{1i}^{+}$ and 7–15 nm (100–220 meV) for $\mathbf{1a}^{+}$ – $\mathbf{1f}^{+}$ (Figure 7).

In the series of tricarbonyl rhenium complexes $\text{fac}[\text{Re}(\text{bpy})(\text{CO})_3(\text{PAR}_3)]^{+}$ (bpy = 2,2'-bipyridine and PAR_3 = triarylphosphine) with π – π and CH– π interactions between the bpy ligand and the aryl groups,¹⁹ similar shifts of the π – $\pi^*(\text{bpy})$ absorption band and $E_{1/2}(\text{bpy}/\text{bpy}^{+})$ were observed in those for $\mathbf{1g}^{+}$ – $\mathbf{1i}^{+}$. It follows that both types of the diimine ligand, i.e., bpy and

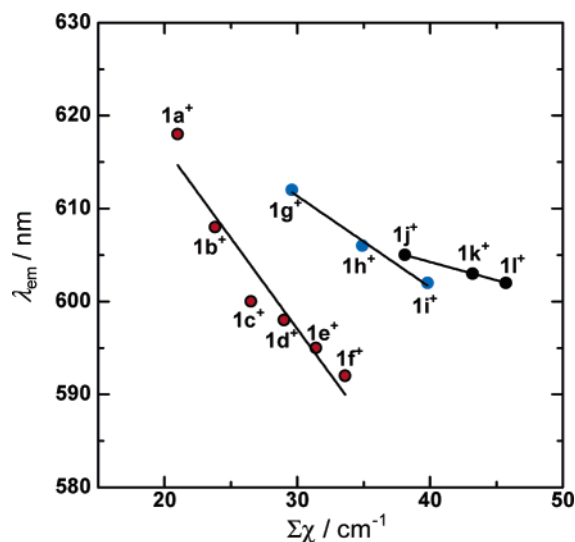


Figure 8. Variations of MLCT emission maxima λ_{em} (in acetonitrile solution at 298 K) with $\Sigma\chi$ values of the PR_3 ligands.

dmb, and of the ligand in the trans position to the triarylphosphine ligand, i.e., CO and $\text{P}(\text{OR})_3$, should not strongly influence the intramolecular interactions. However, the $\text{CH}(\text{phenyl})-\pi(\text{pyridine})-\pi(\text{phenyl})$ interaction has much stronger effects on properties correlated with the dmb ligand.

Effects on the $^3\text{MLCT}$ Excited State. All the rhenium complexes reported here showed strong and unstructured emission from the lowest $^3\text{MLCT}$ excited state at room temperature in solution; an example is shown in Figure 1. Figure 8 illustrates the relation between the emission maximum and $\Sigma\chi$, where dependence on the number of the triarylphosphine ligand(s) in the complex was again observed, and each group of the complexes shows a different relation with $\Sigma\chi$. The pattern is significantly different from that for **MLCT absorption** bands described above (Figure 6): typically, $1\text{c}^+-1\text{f}^+$, with two triarylphosphine ligands, emit with higher energy than the other complexes with one or no triarylphosphine ligand, while the MLCT absorption bands of $1\text{c}^+-1\text{f}^+$ were observed at much lower energy. The $\text{CH}(\text{phenyl})-\pi(\text{pyridine})-\pi(\text{phenyl})$ interactions consequently reduce the MLCT absorption energy but raise the emission energy from the $^3\text{MLCT}$ excited state. In the cases of $1\text{g}^+-1\text{i}^+$, although the emissions were observed at similar wavelength as $1\text{j}^+-1\text{l}^+$, examination of the lower energy MLCT absorptions of $1\text{g}^+-1\text{i}^+$ relative to $1\text{j}^+-1\text{l}^+$ leads to the conclusion that the $\pi-\pi$ and $\text{CH}-\pi$ interactions in $1\text{g}^+-1\text{i}^+$ also cause higher-energy shifts of the emission from their “ordinal” energies. The $\pi-\pi$ and $\text{CH}-\pi$ interactions and the $\text{CH}(\text{phenyl})-\pi(\text{pyridine})-\pi(\text{phenyl})$ interaction consequently decrease the Stokes shifts by ~ 140 and ~ 310 meV, respectively.

The lifetime of the $^3\text{MLCT}$ excited state was also strongly affected by the intramolecular interactions (Table 3): the $\pi-\pi$ and $\text{CH}-\pi$ interactions and the $\text{CH}(\text{phenyl})-\pi(\text{pyridine})-\pi(\text{phenyl})$ interaction increase the emission lifetime (τ_{em}) by about twice and three times, respectively. This variation is dominated by effects of the intramolecular interactions on the nonradiative decay rate from $^3\text{MLCT}$ (k_{nr} in Table 3), whereas the radiative decay rate (k_{r}) did not systematically change.

As described above, the intramolecular interactions red-shift the $^1\text{MLCT}$ absorption band but blue-shift the emission from the $^3\text{MLCT}$ excited state. These “discrepant” phenomena can

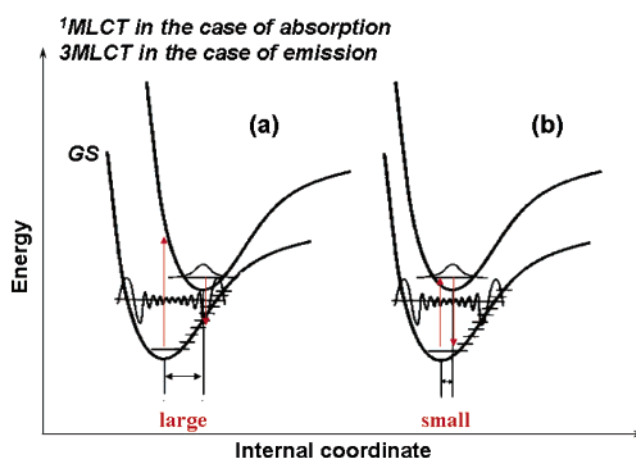


Figure 9. Qualitative illustration of the potential energy curves of the ground state (GS) and metal-to-ligand charge-transfer excited state ($^1\text{MLCT}$ in the case of absorption and $^3\text{MLCT}$ in the case of emission) of *cis,trans*- $[\text{Re}(\text{dmb})(\text{CO})_2(\text{PR}_3)(\text{PR}'_3)]^+$ where (a) R, R' = alkoxy and (b) aryl groups. In both cases the energies of the GS and $^3\text{MLCT}$ are assumed to be identical with each other.

be explained using Figure 9 as follows. Both the $^1\text{MLCT}$ and $^3\text{MLCT}$ excited states of a metal complex usually have different nuclear geometries and solvation from the corresponding ground state, as shown in Figure 9a, because of the differing polarization of the molecule between the ground and excited states.⁷⁴ The intramolecular interactions probably cause the electron located mainly on the dmb ligand in the $^3\text{MLCT}$ excited state to be partially dispersed to the aryl groups and the hydrogen on the phosphorus ligands. This should lower the difference in the polarization between the ground state and the MLCT excited states, reducing the gap between their energy surfaces on the abscissa as shown in Figure 9b. In this situation, the absorption, i.e., the transition from the lowest vibrational level in the ground state to the $^1\text{MLCT}$ excited state, is observed at lower energy, but the emission, i.e., the jump from the lowest vibrational level of $^3\text{MLCT}$ excited to the ground state, is at higher energy. The smaller gap between the ground state and the $^3\text{MLCT}$ excited state may also give rise to smaller Franck–Condon factors, as illustrated in Figure 9b, slowing nonradiative decay.

Another possible explanation for the phenomena involving weak interactions is an “internal solvation” effect of the aryl groups on the phosphine ligands, such that when the dmb ligand is between two hydrophobic aryl groups, the local environment around the bpy ligand has a lower regional dielectric constant than others. This hydrophobic environment could cause the MLCT excited state to be unstable, so that emission is blue-shifted. This cannot, however, explain the positive shift of the reduction potential and the red-shift of the $^1\text{MLCT}$ absorption band.

Figure 10 shows T–T absorption spectra of 1e^+ , 1h^+ , and 1k^+ measured 20 ns after a laser flash. The broad absorption band at 420–600 nm is attributable to the (dmb^-) ligand localized excitation in the $^3\text{MLCT}$ excited state. The absorption of $(1\text{e}^+)^*$ with two triarylphosphine ligands was broader, and its λ_{max} was red-shifted by 26 nm relative to that of $(1\text{k}^+)^*$ without triarylphosphine. This also suggests that the $\text{CH}(\text{phenyl})-\pi(\text{pyridine})-\pi(\text{phenyl})$ interaction is maintained in the excited state of the complexes with two triarylphosphines. The

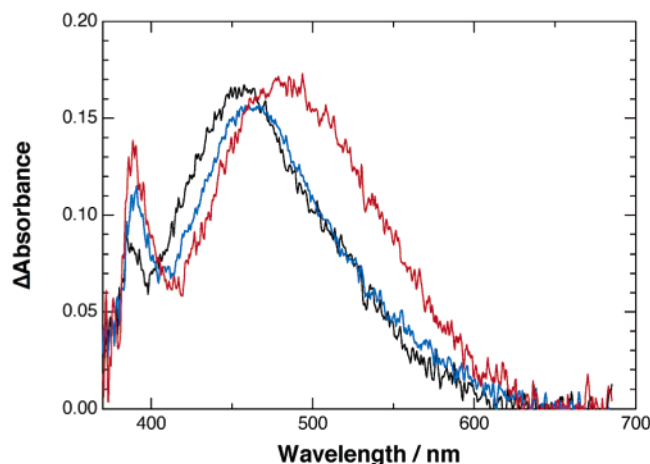


Figure 10. T-T Absorption spectra of $1e^+$ (red), $1h^+$ (blue), and $1k^+$ (black) measured 20 ns after a laser flash (355 nm). The solvent was acetonitrile, and the absorbance changes (Δ absorbance) were corrected by the relative absorption light quanta of the sample solutions.

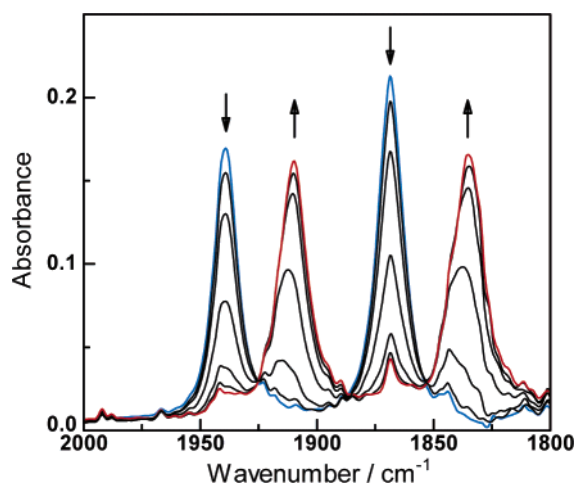


Figure 11. IR spectral change in the ν_{CO} region by flow electrolysis of $1e^+$ (0.5 mM) in Ar-saturated acetonitrile solution containing 0.1 M Et_4NBF_4 . The complex was reduced at 0 V to -1.96 V vs $Ag/AgNO_3$ at a constant flow rate of 0.5 mL/min.

T-T absorption of $(1h^+)^*$ with one triarylphosphine ligand was also red-shifted, but the difference was 6 nm compared with $(1k^+)^*$.

Effects on One-Electron-Reduced Species of the Complexes. In most systems using a rhenium(I) diimine complex as photocatalyst or electrocatalyst, the one-electron-reduced (OER) species of the complex, where the added electron is mainly located in the diimine ligand, is an important intermediate produced by reductive quenching of the 3MLCT excited state of the complex^{9,10,18a,24,25} or electrochemical reduction.^{3,26} We investigated the effects of the intramolecular interactions on properties of the OER species of the rhenium complexes.

Figure 11 shows the IR spectra in the ν_{CO} region of an acetonitrile solution containing $1e^+$ and an electrolyte after flow electrolysis^{18a} at various potentials. A set of observed isosbestic points and results of coulometric measurements clearly show

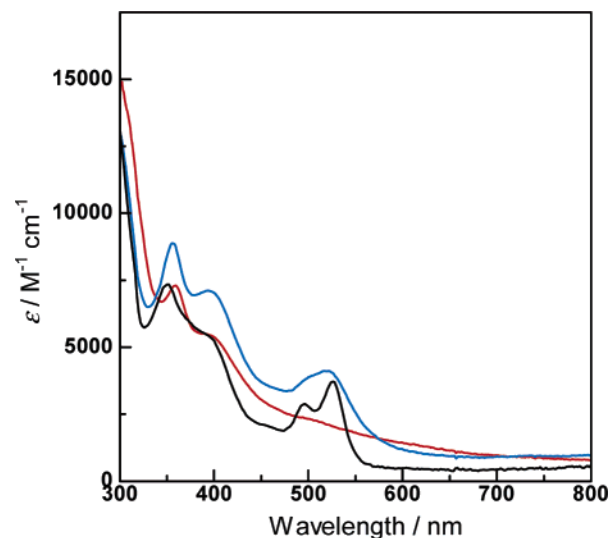


Figure 12. UV/vis absorption spectra of the one-electron-reduced (OER) species produced using flow electrolysis in Ar-saturated acetonitrile solution containing 0.1 M Et_4NBF_4 at room temperature: $1e$ (red), $1h$ (blue), and $1j$ (black).

that a one-electron-reduced (OER) species, i.e., $1e$, was produced by the electrolysis and remained stable during spectrum measurement. The ν_{CO} bands of $1e$ were shifted to lower frequency relative to those of $1e^+$ (Table 4). Such shifts are usually observed in one-electron reduction of rhenium(I) diimine complexes, because stronger π -back-donation from the Re to the antibonding π^* orbital of the CO ligands, which was promoted by higher electron density on the (dmb^-) ligand, weakens the CO bonds.^{3,10b,18a} Similar IR spectral changes were observed for the electrochemical reduction of $1a^+$, $1c^+$, $1f^+$, $1h^+$, and $1j^+$. Table 4 summarizes the principal and interaction force constants k_{CO} and $k_{CO,CO}$ and their differences (Δk_{CO} and $\Delta k_{CO,CO}$) between the OER species and their parent complexes. The similarity in Δk_{CO} and $\Delta k_{CO,CO}$ for all measured rhenium complexes clearly indicates that the electron density on the $d\pi$ orbitals of the central rhenium is predominantly affected by the phosphorus ligands through the Re–P bonds in the OER species.

On the other hand, UV/vis absorption spectra of OER species with one or two triarylphosphine ligands were dramatically different from those with none. Figure 12 shows three typical examples, i.e., $1j$, $1h$, and $1e$, in which the phosphorus ligands have similar χ values. The spectrum of $1j$ has common characteristics with spectra of various *fac*-[Re(LL $^-$)(CO) $_3$ -(L')] $^{n+}$ - and *cis,trans*-[Re(LL $^-$)(CO) $_2$ {P(OR) $_3$ }(L')] $^{n+}$ -type complexes (LL = bpy and its derivatives; L' = monodentate ligand; $n = 0$ or 1),^{10a,b,18} the vibrational bands were observed at 480–540 nm. This electronic transition is attributed to ligand (dmb^-) -centered excitation. The corresponding band of $1h$ with a triphenylphosphine ligand was, on the other hand, nonvibrational and broad. In the spectrum of $1e$ with two tri(4-fluorophenyl)-phosphine ligands, no absorption maximum was seen around 500 nm, and the absorption extended to 800 nm. The spectra of $1a$ and $1c$ were very similar to those of $1e$. These results strongly suggest that the intramolecular interactions between the *dmb* ligand and the triarylphosphine ligand(s) are maintained, and probably enhanced, in the OER species. It is reasonable to suppose that the extra electron residing in the π^* orbital of the *dmb* ligand is partially dispersed to the aryl groups on the triarylphosphine ligand(s), as in the 3MLCT excited state.

- (24) Kutal, C.; Corbin, A. J.; Ferraudi, G. *Organometallics* **1987**, 6, 553–557.
 (25) Kalyanasundaram, K. *J. Chem. Soc., Faraday Trans. 2* **1986**, 82, 2401–2415.
 (26) (a) Sullivan, B. P.; Bolinger, C. M.; Conrad, D.; Vining, W. J.; Meyer, T. *J. J. Chem. Soc., Chem. Commun.* **1985**, 1414–1416. (b) Hayashi, Y.; Kita, S.; Brunschwig, B. S.; Fujita, E. *J. Am. Chem. Soc.* **2003**, 125, 11976–11987.

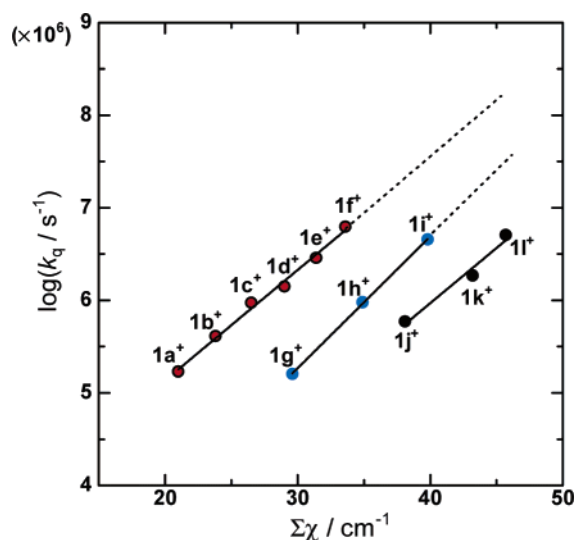


Figure 13. Relation between the quenching rate constant k_q of the emission from the excited 1^+ by TEOA and $\Sigma\chi$ value of the PR_3 ligands.

Effects on the Photochemical Electron Transfer and Photocatalysis of the Rhenium Complexes. We expect that the intramolecular interactions increase the oxidation power of the rhenium complex in the $^3\text{MLCT}$ excited state, as well as in the ground state, even though the $^1\text{MLCT}$ absorption band is red-shifted. This is because of the positive shift in the reduction potential of the complex in the ground state and of the blue shift of the emission from the complex in the $^3\text{MLCT}$ excited state. Figure 13 shows the relation between $\Sigma\chi$ and the quenching rate constant of the emission from the excited 1^+ by triethanolamine (TEOA), which has been often used as a sacrificial electron donor in photocatalytic CO_2 reduction using various rhenium complexes.^{9,10} As expected, different lines can be drawn for each group, including complexes with no triarylphosphine ligand, with one, and with two. From Figure 13, acceleration of the quenching is estimated at ~ 5 times for the $\text{CH}-\pi$ and $\pi-\pi$ interactions and ~ 35 times for the $\text{CH}(\text{phenyl})-\pi(\text{pyridine})-\pi(\text{phenyl})$ interactions. In photocatalytic CO_2 reduction using rhenium complexes, a mixed solution of 1:5 (v/v) TEOA–dimethylformamide has been often used. In this solution the quenched fraction of the excited 1^+ , η_q obtained using eq 8 where I and I_0 are the respective emission intensities in the presence and absence of TEOA, varied with both electronic properties of the phosphorus ligands and the intramolecular interactions, as shown in Figure 14. The intramolecular interactions can cause a red-shift of the $^1\text{MLCT}$ absorption band of complexes with the same η_q value, up to 50 nm.

$$\eta_q = \frac{I_0 - I}{I_0} \times 100 \quad (8)$$

Table 8 summarizes photocatalyses of 1^+ for CO_2 reduction. Only those complexes with the $\text{CH}(\text{phenyl})-\pi(\text{pyridine})-\pi(\text{phenyl})$ interactions $1\text{a}^+ - 1\text{f}^+$ can photocatalyze CO_2 reduction to give CO. Since the photocatalytic reactions are initiated by the reductive quenching process of the $^3\text{MLCT}$ excited state of 1^+ by TEOA, the intramolecular interaction should facilitate this process, as described above.

The other complexes had low or no photocatalytic ability in this reaction condition. The reason for this difference is not yet

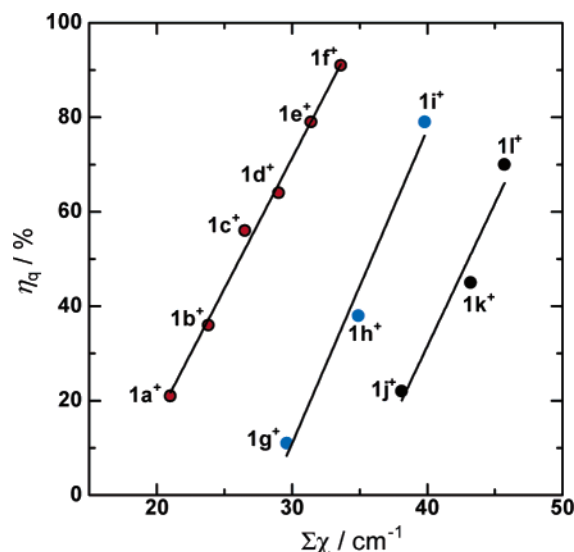


Figure 14. Relation between the quenched fraction η_q of the excited 1^+ and $\Sigma\chi$ value of the PR_3 ligands in 4 mL of TEOA–DMF (1:5 v/v) solution at room temperature.

Table 8. Photocatalytic Reduction of CO_2 Using 1^+ as Photocatalyst

complex	TN_{CO}^a	Φ_{CO}^b	$\eta_q^c/\%$
1a^+	2.3	0.01	21
1b^+	4.6	0.07	36
1c^+	6.8	0.16	56
1d^+	13.1	0.19	64
1e^+	17.3	0.20	79
1f^+	10.6	0.22	91
1g^+	0.5	0.02	11
1h^+	0.6	0.05	38
1i^+	1.4	0.09	79
1j^+	0.2	0.02	22
1k^+	0.2	0.06	45
1l^+	1.0	0.12	70

^a Turnover number of CO formation based on the complex used (0.5 mM). ^b Quantum yield for CO formation. 4 mL of DMF–TEOA (1.26 M) solution containing the complex (2.0 mM) was irradiated at 365 nm. Light intensity was 8.22×10^{-9} einstein s^{-1} for 1a^+ , 1c^+ , 1e^+ , 1f^+ , 1h^+ , and 1j^+ , and 5.24×10^{-9} einstein s^{-1} for 1b^+ , 1d^+ , 1g^+ , 1i^+ , 1k^+ , and 1l^+ . Error $\pm 10\%$. ^c Reductive-quenching efficiency of the $^3\text{MLCT}$ excited states of 1^+ by TEOA (1.26 M).

clear, because the reaction mechanism of photocatalytic reduction of CO_2 using rhenium complexes has not been settled. However, there are some significant experimental results. It has been reported that reaction of OER species produced by reductive quenching with CO_2 is a significant process in *fac*- $[\text{Re}^{\text{I}}(\text{X}_2\text{bpy})(\text{CO})_3\text{PR}_3]^+$ -photocatalytic reduction of CO_2 , which proceeds efficiently when $E_{1/2}^{\text{red}}$ for the complex is more negative than -1.4 V vs Ag/AgNO_3 .^{10b} All of the complexes 1^+ satisfy this requirement, as shown in Table 5. Stability of the OER species is also important for CO_2 reduction photocatalysts. For example, *fac*- $[\text{Re}(\text{bpy})(\text{CO})_3\text{L}]^+$ ($\text{L} = \text{pyridine}$ and PPh_3) cannot work as photocatalyst for CO_2 reduction because of instability of their OER species, from which loss of L initiates a chain reaction of decomposition of the parent complex.^{10c,27} During the photocatalytic reaction, much faster decomposition of $1\text{g}^+ - 1\text{i}^+$ with one triarylphosphine ligand was observed than with the other complexes. Figure 15b shows a

(27) Hori, H.; Ishihara, J.; Koike, K.; Takeuchi, K.; Ibusuki, T.; Ishitani, O. *J. Photochem. Photobiol., A: Chem.* **1999**, *120*, 119–124.

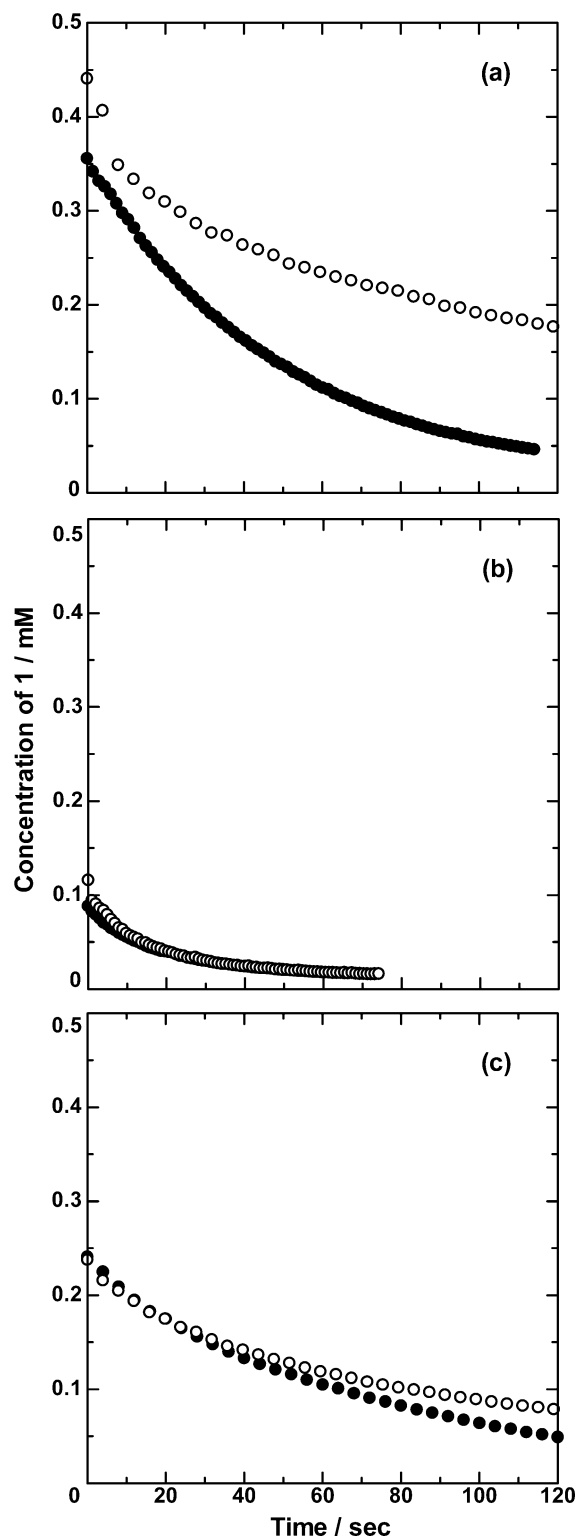
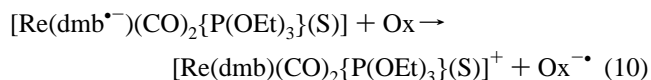
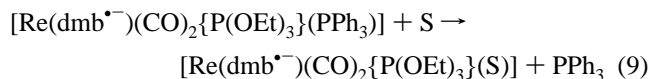


Figure 15. Decay curves of the OER species of (a) **1e⁺**, (b) **1h⁺**, and (c) **1j⁺**, produced by the photochemical reduction by TEOA using 365-nm light in 4 mL of TEOA–DMF (1:5 v/v) solution at room temperature, under Ar atmosphere (○) or under CO₂ atmosphere (●). The sample concentration was 0.5 mM.

decay curve of **1h** produced by photochemical reduction of **1h⁺** using TEOA. Decay under Ar atmosphere (open circles) was much faster than for the other types of the complexes such as

1e and **1j** (Figure 15a and c), and the presence of CO₂ in the reaction solution (closed circles) did not increase the decay rate, implying that **1h** has too short a lifetime to react with CO₂ because it decomposes to give the corresponding solvento complexes [Re(dmb)(CO)₂{P(OEt)₃}(S)]⁺ (S = DMF and TEOA) probably via eqs 9 and 10, where Ox = [Re(dmb)-(CO)₂{P(OEt)₃}(PPh₃)]⁺ or other oxidants.



This is likely to be a main reason for the low photocatalysis of **1h⁺**, and probably also for **1g⁺** and **1i⁺**. Both of the other OER species **1e** and **1j** were relatively stable under Ar atmosphere but decayed faster under CO₂, where the pseudo-first-order rate constants were, respectively, 0.016 and 0.013 s⁻¹. We do not have any experimental data about the properties of the CO₂ adducts produced from the OER species, which might strongly affect the photocatalytic reactions.

Conclusion

Intramolecular interactions, especially CH(phenyl)–π(pyridine)–π(phenyl) interactions, between the dmb ligand and the triarylphosphine ligand(s), have striking and unique effects on the various properties associated with the dmb ligand in the ground state, in the excited state, and in the one-electron-reduced state. Typical examples are summarized in Table 1, in which the complexes with similar Σχ values (**1e⁺**, **1h⁺**, and **1j⁺**) can be compared with each other. The interactions cause the UV/vis absorptions to both π–π* and ¹MLCT to be red-shifted, but the emission from ³MLCT is blue-shifted, the lifetime of the ³MLCT excited state is prolonged, the oxidation power in both the ground and excited states is enhanced, and photocatalysis for CO₂ reduction is also enhanced. Moreover, properties associated with the central rhenium, specifically the electron densities on the dπ orbitals, are much less affected by the interactions or are unaffected. These unique characteristics of the intramolecular interactions give a novel and potentially useful method to control the photophysical, photochemical, and electrochemical functions of metal complexes.

Acknowledgment. We are grateful thanks to Dr. Koichi Nozaki of the Osaka University for his helpful discussion. This work was partly supported by a Grant-in-Aid for Scientific Research No. 17036015 on Priority Areas (434:Chemistry of Coordination Space) from the Ministry of Education, Culture, Sports, Science and Technology of Japan, and CREST, Japan Science and Technology Agency.

Supporting Information Available: X-ray crystallographic files (CIF) of **1e⁺**, deviations of the atoms constructing the pyridine rings of the dmb ligand from their best planes in the crystals of **1e⁺**CF₃SO₃⁻ and **1h⁺**PF₆⁻. This material is available free of charge via the Internet at <http://pubs.acs.org>.

JA053814U